

How Many ENSO Flavors Can We Distinguish?*

NATHANIEL C. JOHNSON

International Pacific Research Center, School of Ocean and Earth Science and Technology, University of Hawaii at Manoa, Honolulu, Hawaii

(Manuscript received 2 September 2012, in final form 27 December 2012)

ABSTRACT

It is now widely recognized that El Niño–Southern Oscillation (ENSO) occurs in more than one form, with the canonical eastern Pacific (EP) and more recently recognized central Pacific (CP) ENSO types receiving the most focus. Given that these various ENSO “flavors” may contribute to climate variability and long-term trends in unique ways, and that ENSO variability is not limited to these two types, this study presents a framework that treats ENSO as a continuum but determines a finite maximum number of statistically distinguishable representative ENSO patterns. A neural network–based cluster analysis called self-organizing map (SOM) analysis paired with a statistical distinguishability test determines nine unique patterns that characterize the September–February tropical Pacific SST anomaly fields for the period from 1950 through 2011. These nine patterns represent the flavors of ENSO, which include EP, CP, and mixed ENSO patterns. Over the 1950–2011 period, the most significant trends reflect changes in La Niña patterns, with a shift in dominance of La Niña–like patterns with weak or negative western Pacific warm pool SST anomalies until the mid-1970s, followed by a dominance of La Niña–like patterns with positive western Pacific warm pool SST anomalies, particularly after the mid-1990s. Both an EP and especially a CP El Niño pattern experienced positive frequency trends, but these trends are indistinguishable from natural variability. Overall, changes in frequency within the ENSO continuum contributed to the pattern of tropical Pacific warming, particularly in the equatorial eastern Pacific and especially in relation to changes of La Niña–like rather than El Niño–like patterns.

1. Introduction

El Niño–Southern Oscillation (ENSO) is the dominant mode of tropical atmosphere–ocean interaction on interannual time scales, with impacts that span much of the globe (Ropelewski and Halpert 1987; Trenberth and Caron 2000). Typically, ENSO episodes have been identified through the monitoring of sea surface temperature (SST) anomalies in the equatorial Pacific region, most notably the so-called Niño-3.4 region (5°S–5°N, 120°–170°W). However, recent studies have made it increasingly clear that traditional definitions of ENSO episodes fail to distinguish two unique types of El Niño episode, the canonical El Niño that is centered in the eastern equatorial Pacific and the more recently recognized

El Niño that is centered farther west near the International Date Line. This latter type, which has been referred by various names such as the “dateline El Niño” (Larkin and Harrison 2005), “El Niño Modoki” (Ashok et al. 2007), “warm pool El Niño” (Kug et al. 2009), and “central Pacific El Niño” (Yeh et al. 2009), has received increased attention because of its unique underlying dynamics (Kao and Yu 2009; Kug et al. 2009; Newman et al. 2011a,b; Yu and Kim 2011), global impacts (Larkin and Harrison 2005; Weng et al. 2007; Ashok et al. 2007; Mo 2010; Hu et al. 2012), and potential trends under global warming (Yeh et al. 2009) relative to those of the eastern Pacific (EP) El Niño. On the basis of climate model simulations analyzed in the Intergovernmental Panel on Climate Change Fourth Assessment Report (IPCC AR4), Yeh et al. (2009) suggest that the relative frequency of central Pacific (CP) El Niño episodes may increase under anthropogenic global warming in response to changes in the equatorial Pacific mean thermocline. However, the recent increasing trend in the frequency of CP El Niño episodes (Lee and McPhaden 2010) may be indistinguishable from natural variability (Newman et al. 2011b; Yeh et al. 2011).

* International Pacific Research Center Publication Number 941 and School of Ocean and Earth Science and Technology Publication Number 8821.

Corresponding author address: Nathaniel Johnson, IPRC, University of Hawaii at Manoa, 401 POST Building, Honolulu, HI 96822.
E-mail: natj@hawaii.edu

The recent focus on the distinction between the EP and CP El Niño is consistent with the notion that ENSO may come in many different “flavors” (Trenberth and Stepaniak 2001) that are distinct from the canonical El Niño and La Niña composites and cannot be characterized by a single index. To describe the structure and evolution of these various flavors, investigators have increasingly considered multiple indices that capture the zonal gradient of equatorial Pacific SST anomalies such as the “Trans-Niño Index” (Trenberth and Stepaniak 2001) or, more commonly for the identification of EP and CP El Niño episodes, a comparison between Niño-3 (5°S–5°N, 150°–90°W) and Niño-4 region (5°S–5°N, 160°E–150°W) SST anomalies. Although this additional information clearly reveals some of the distinct properties between various ENSO episodes, such subjective index choices are not necessarily optimal for describing the various ENSO flavors that are discernible in the observational record.

Another common approach for distinguishing tropical SST patterns is through empirical orthogonal function (EOF) analysis, but this method is not guaranteed to reveal physically interpretable SST modes (e.g., L’Heureux et al. 2013). In particular, the leading EOF of tropical Pacific SSTs generally resembles the canonical EP ENSO pattern, and either the second (e.g., Ashok et al. 2007) or third (e.g., L’Heureux et al. 2013) EOF resembles the CP ENSO pattern. However, this second or third EOF also tends to capture the spatial asymmetry between the EP El Niño and La Niña patterns (Hoerling et al. 1997; Rodgers et al. 2004), which means that this particular EOF is not uniquely identified with CP ENSO episodes. This complication highlights one of the potential pitfalls of using a linear, orthogonal method such as EOF analysis to characterize nonlinear, nonorthogonal SST patterns.

In this study, we consider a new perspective and methodology for describing ENSO flavors. Under the perspective presented here, we recognize that there is a continuum of ENSO states but that the relatively brief observational record limits the number of distinct ENSO flavors that we can distinguish. Here we consider a methodology that treats ENSO as a continuum but also determines a finite maximum number of statistically distinguishable ENSO flavors. This approach is based on a pairing of a type of neural network–based cluster analysis, called self-organizing map (SOM) analysis, with a statistical distinguishability test, described more thoroughly in the following section. This approach represents a more objective partitioning of the equatorial Pacific SST data than the standard approach of partitioning by somewhat subjective SST indices. In addition, this approach, which is constrained by neither linearity nor orthogonality, avoids the disadvantages of common

linear methods such as EOF analysis and often results in more easily interpretable physical patterns (Reusch et al. 2005; Liu et al. 2006; Johnson et al. 2008).

Because tropical SST trends play a critical role in remote regional temperature and precipitation trends (Shin and Sardeshmukh 2011) and tropical precipitation and circulation changes (Xie et al. 2010; Johnson and Xie 2010; Ma et al. 2012; Tokinaga et al. 2012), it is worthwhile to examine how changes in the frequency of different ENSO flavors impact the long-term SST trend. As demonstrated and discussed in the following three sections, the framework adopted here allows us to connect the long-term SST trend to changes in the frequency distribution of interannually varying SST patterns.

The remainder of the paper is organized as follows. Section 2 provides a description of the general framework, methodology, and data used in this analysis. Section 3 presents the main results, which include the SOM cluster patterns and the results of the trend analysis. The paper concludes with discussion and conclusions in sections 4 and 5.

2. Data and methodology

In this section we examine the approach for determining the ENSO region SST clusters and then determining the maximum number of distinguishable clusters.

a. Self-organizing map SST cluster patterns

Conceptually, we would expect that determining the maximum number of distinguishable ENSO flavors would require a partitioning of tropical Pacific SST fields into groups that maximize similarity within groups while also maximizing the dissimilarity between groups. Computationally, this sort of partitioning may be accomplished either by K -means cluster or SOM analysis. Specifically, K -means cluster analysis treats each SST field as an M -dimensional vector, where M is the number of grid points, and minimizes the sum of squared distances between each SST field and the nearest of the K cluster centroids. There are several reasonable choices for a distance metric, but Euclidean distance is perhaps most commonly used, and is used in the analysis presented here. The clusters are most commonly determined through an iterative, two-step procedure described as follows: Given an initial assignment of K cluster centroids, which may be a random distribution, the first step is the assignment of the data vectors (SST fields in this case) to the nearest cluster centroid, and the second step is the calculation of the new cluster centroids. These two steps are repeated until the cluster assignments no longer change, which corresponds to a local minimum of the sum of squared distances described above.

The value of K must be specified prior to the cluster analysis, and the method for determining K for this problem is discussed in section 2b. K -means cluster analysis has remained a popular method of cluster analysis in the atmospheric and ocean sciences for decades (e.g., Michelangeli et al. 1995; Christiansen 2007; Johnson and Feldstein 2010; Riddle et al. 2013; Freeman et al. 2012).

SOM analysis (Kohonen 2001) is a relatively new neural network–based cluster analysis that bears strong similarities to K -means clustering and has increased in popularity in the atmospheric and ocean sciences over the past decade (e.g., Hewitson and Crane 2002; Richardson et al. 2003; Liu et al. 2006; Leloup et al. 2007; Johnson et al. 2008; Jin et al. 2010; Lee et al. 2011; Chu et al. 2012). SOM analysis most significantly distinguishes itself from K -means cluster analysis through the addition of a topological ordering on a low-dimensional (typically one- or two-dimensional) map. In other words, the clusters “self organize” such that similar clusters are located close together on this low-dimensional map, often displayed as a grid, and dissimilar clusters are located farther apart. This combination of clustering and topological ordering makes SOM analysis effective for providing a visualization of the continuum of patterns within a dataset. Similar to the objectives of this study, SOM analysis has been used in previous studies to describe the continuum of atmospheric teleconnection patterns (e.g., Johnson et al. 2008; Lee et al. 2011) and to describe decadal changes in ENSO (Leloup et al. 2007).

The self-organizing nature of SOM analysis owes to a component called the neighborhood function, with an associated parameter called the *neighborhood radius*. When the neighborhood radius is greater than zero, the clusters become organized within the low-dimensional map. When the neighborhood radius is set to zero, the SOM algorithm reduces to the K -means clustering algorithm. Thus, SOM analysis can be considered a “constrained version of K -means clustering” (Hastie et al. 2009). In the present analysis, a one-dimensional SOM analysis is performed such that the neighborhood radius gradually shrinks to a value of zero. Therefore, the SOM patterns become topologically ordered along a line when the neighborhood radius is greater than zero, but the algorithm used to determine the cluster patterns converges to the K -means clustering algorithm. The SOM approach is chosen to ensure that similar ENSO flavors are grouped together, but we would expect to see similar results with K -means cluster analysis. See the appendix of Johnson et al. (2008) for a more thorough description of the basic SOM methodology and Liu et al. (2006) for additional information on recommended SOM parameter choices.

In this study, we consider ENSO flavors to be represented by SOM SST anomaly patterns in the equatorial Pacific domain. We use September–February mean SST data for the period from 1950 through 2011 derived from the Extended Reconstructed Sea Surface Temperature Dataset, version 3b (ERSST.v3b; Xue et al. 2003; Smith et al. 2008). The September–February period is used because of the seasonal phase locking of ENSO, which results in the vast majority of ENSO episodes peaking during boreal fall or winter. The starting year of 1950 is chosen because of the improved spatial and temporal coverage of SST data that begins around that time (Deser et al. 2010; see their Fig. 3). In addition, prior to 1950 the SST patterns of ENSO episodes may depend strongly on the method of reconstruction for the SST dataset (Giese and Ray 2011; Ray and Giese 2012). The chosen domain covers the tropical Pacific region between 120°E and 50°W and between 25°S and 25°N. The ERSST.v3b data are on a 2° latitude–longitude grid, but because the analysis described in the following section requires equal weight to be placed on each grid point, the data are linearly interpolated to an equal-area grid with 1° latitudinal spacing and longitudinal spacing that increases from 1° at the equator to approximately 1.1° at 25° latitude. Anomalies are calculated by subtracting the seasonal cycle for the 1981–2010 base period. The choice of the most recent 30-yr climatology is based on the standard practice of the National Oceanic and Atmospheric Administration (NOAA) Climate Prediction Center (CPC), but the focus of this study, the spatial variations and trends of ENSO flavors, is not sensitive to this choice of base period. SOM analysis is performed on the SST anomaly data for various choices of K , as described in section 2b. Because the analysis converges to a local rather than global minimum of the error function described at the beginning of this section, the SOM analyses and all tests of section 2b are repeated five times without any noticeable change in results. Thus, the results presented here are robust. All SOM calculations are performed with the Matlab SOM Toolbox (Vesanto et al. 2000), which is freely available on the web (<http://www.cis.hut.fi/somtoolbox/>).

b. Determining the maximum number of distinguishable ENSO flavors

Because K must be specified prior to a K -means cluster or SOM analysis, one challenge in any cluster analysis is the determination of the optimal number of clusters. Many studies have suggested various useful heuristic methods for determining K (e.g., Michelangeli et al. 1995; Christiansen 2007; Hastie et al. 2009; Riddle et al. 2013), but an objective optimal K has remained elusive. In this study, we consider a new criterion for choosing K : the maximum number such that all clusters are statistically

distinguishable from another. Thus, if K^* is the optimal K by this criterion, then we can determine K^* unique cluster patterns, but $K^* + 1$ clusters would result in two or more clusters that are indistinguishable by this statistical definition. In the present application, K^* would refer to the maximum number of statistically discernible ENSO flavors.

The determination of whether two cluster patterns are statistically distinguishable requires a test of field significance. Often times in the atmospheric and ocean sciences, field significance tests have been conducted through Monte Carlo resampling methods (Livezey and Chen 1983). Recently, another field significance approach based on the “false discovery rate” (FDR) has been introduced to the climate sciences (Benjamini and Hochberg 1995; Wilks 2006). The FDR refers to the expected proportion of local null hypotheses that are rejected but are actually true. In the present application, the local hypotheses being evaluated are whether the SST anomalies at each grid point in cluster pattern i are significantly different from the corresponding SST anomalies in cluster pattern j . If at least one local test has a p value that satisfies the specified FDR criterion, typically $q = 0.05$, then the cluster patterns are statistically distinguishable also at the level q . If no local tests meet the FDR criterion, then the cluster patterns are statistically indistinguishable. Further explanation of this test is provided below. The FDR approach has a number of advantages over conventional field significance tests, including generally better test power, robust results even when the local test results are correlated with each other, and the identification of significant local tests while controlling the proportion of false rejections (Wilks 2006). In addition, FDR tests are much more computationally efficient than Monte Carlo methods, and so a large number of field significance tests can be conducted with little computational effort, as required for the tests described here.

To determine if SOM cluster i is statistically distinguishable from SOM cluster j , we first calculate the p values (two-sided) at each grid point corresponding to the Student’s t distribution for a difference of means, where the null hypothesis is that the local SST composite anomalies are the same in both clusters. This test is based on the recognition that SOM cluster pattern i (j) with n_i (n_j) cluster members is equivalent to an SST composite pattern with n_i (n_j) samples that comprise the composite.¹ Each of the n_i or n_j cluster members is

a seasonal SST anomaly field assigned to that cluster on the basis of minimum Euclidean distance. For each pair of cluster pattern composites, we calculate the p values corresponding to

$$t(\lambda, \theta) = \frac{\overline{\text{SST}}_i(\lambda, \theta) - \overline{\text{SST}}_j(\lambda, \theta)}{S(\lambda, \theta) \sqrt{\frac{1}{n_i} + \frac{1}{n_j}}}, \quad (1)$$

where

$$S(\lambda, \theta) = \sqrt{\frac{(n_i - 1)S_i(\lambda, \theta)^2 + (n_j - 1)S_j(\lambda, \theta)^2}{n_i + n_j - 2}}. \quad (2)$$

The variable $\overline{\text{SST}}_i$ ($\overline{\text{SST}}_j$) signifies the composite SST anomaly for SOM cluster i (j), and S_i (S_j) indicates the standard deviation corresponding to all SST anomalies within cluster i (j) at latitude λ and longitude θ . For these calculations, we assume that each SST anomaly field represents an independent sample, which is reasonable for seasonal fields separated by at least a year and usually several years within each cluster.

The calculations for a pair of cluster patterns described above result in a distribution of a number M local p values, where, again, M is the total number of grid points. If all M local null hypotheses are true, and if the results of the local tests are independent of each other, then the resulting M local p values will be a random sample from the uniform distribution $U(0, 1)$ (e.g., Folland and Anderson 2002; Wilks 2006). If some of the local null hypotheses are false, then the corresponding p values will be smaller than expected from this uniform distribution. The FDR test evaluates the distribution of p values to determine the local p value that provides confidence in the correct rejection of local null hypotheses; that is, the p value that controls the FDR at the level q , which is also the global or field significance level α_{global} . This test is conducted as follows. Let $p_{(m)}$ denote the m th smallest of the M local p values. The FDR can be controlled at the level q for

$$p_{\text{FDR}} = \max_{m = 1, \dots, M} \left[p_{(m)} : p_{(m)} \leq q \left(\frac{m}{M} \right) \right]. \quad (3)$$

All local tests that yield a p value less than or equal to the largest p value that satisfies the right-hand side of (3) are deemed significant, which means that the expected fraction of local null hypotheses that are actually true for those tests is less than or equal to q . If no local tests meet the criterion specified in (3), then the patterns are statistically indistinguishable. In the present application,

¹ The equivalence between SOM cluster patterns and composites is strictly true only when the neighborhood radius of the SOM algorithm is equal to zero, as specified as the final radius in this analysis. This equivalence is always true for K -means cluster analysis.

we shall not focus on the specific value of p_{FDR} but instead shall focus on whether or not any local tests satisfy (3) for $q = 0.05$ —that is, whether or not the cluster patterns are statistically distinguishable at the 5% level. Although the assumption of independent local tests does not hold in this case because of the high spatial correlation in the SST fields, the results of FDR tests do not appear sensitive to this independence assumption (Wilks 2006).

For K SOM cluster patterns there are $K(K - 1)/2$ possible pairs of patterns to compare with the test described above. To determine K^* , we perform the SOM analysis for values of K that increase from 2 to 20 at an increment of 1, perform the $K(K - 1)/2$ field significance tests, as described above, for each choice of K , and count the number of SOM cluster pattern pairs that are statistically indistinguishable. The maximum number of statistically distinguishable ENSO flavors K^* is the largest value of K with zero statistically indistinguishable cluster pattern pairs.

3. Results

We first examine the results of the field significance tests described above. Figure 1 illustrates the number of statistically indistinguishable cluster pattern pairs as a function of K . We see that as K is increased from two to nine, all pairs of cluster patterns for each K remain statistically distinguishable. When K is increased to 10, however, the number of statistically indistinguishable pairs rises above zero. As we would expect, the number of indistinguishable pairs rises monotonically with K above nine.² Thus, by the reasoning stated above, the maximum number of statistically distinguishable ENSO flavors is determined to be nine.

The value of K^* may vary slightly based on the domain chosen to represent ENSO flavors. Reasons for the slight variations include changes in the number of spatial degrees of freedom, the convergence of cluster analyses to local rather than global minima of the error functions, and the use of a sharp significance threshold of $\alpha_{\text{global}} = 0.05$. However, we do obtain the same value of K^* when we change the northern and southern boundaries to 20°N and 20°S or move the western boundary to 90°E. Moreover, the analysis performed on both smaller and larger domains results in similar interpretations of the

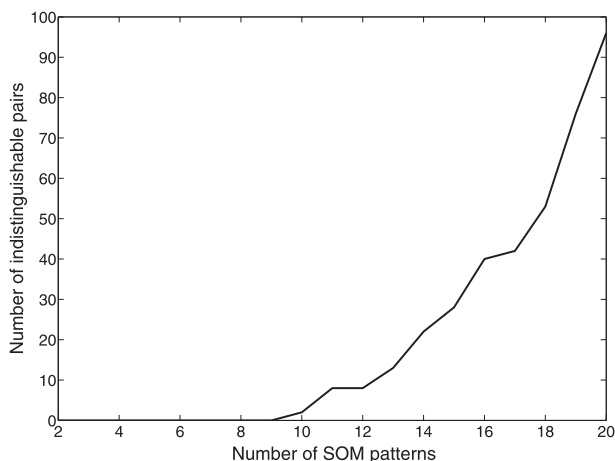


FIG. 1. The number of SOM SST cluster pattern pairs that are statistically indistinguishable at the 5% significance level as a function of the number of SOM patterns K .

variability and trends, supporting the robustness of the results discussed below.

a. SOM of tropical Pacific SST patterns

With K^* determined, we now examine the nine SOM cluster patterns of tropical Pacific SST anomalies. Figure 2 presents these nine patterns for the one-dimensional SOM. Because of the topological ordering by the SOM, similar patterns are similarly numbered. Figure 2 reveals three moderate to strong La Niña-like patterns (patterns 1–3), two weak La Niña-like patterns (patterns 4–5), two weak CP El Niño-like patterns (patterns 6–7), a moderate CP–EP El Niño-like pattern (pattern 8), and a strong EP El Niño-like pattern (pattern 9). In addition to amplitude, La Niña-like patterns most significantly distinguish themselves by the longitude of maximum equatorial cooling and by the presence of weak (pattern 1), negative (patterns 2 and 5), or positive (patterns 3 and 4) western Pacific SST anomalies. El Niño-like patterns also distinguish themselves by amplitude and the longitude of maximum equatorial SST anomalies, but the western Pacific SST anomalies are similar for each El Niño-like pattern. Pattern 9 resembles the canonical EP El Niño, whereas pattern 8 seemingly represents a hybrid EP–CP El Niño pattern, with maximum warming in the central Pacific but a tongue of positive SST anomalies that extends to the South American coast. Together, these nine SST patterns represent the ENSO SST continuum.

As mentioned above, each September–February SST field is assigned to the best-matching SOM pattern on the basis of minimum Euclidean distance. The frequency of occurrence of each SOM pattern is indicated to the bottom right of each map, revealing that most

² If an SOM cluster has only a single member, then (1) is undefined, and the distinguishability test cannot be conducted. Therefore, in cases where a cluster only has one member, all pairs that include that particular cluster are automatically assigned as statistically indistinguishable.

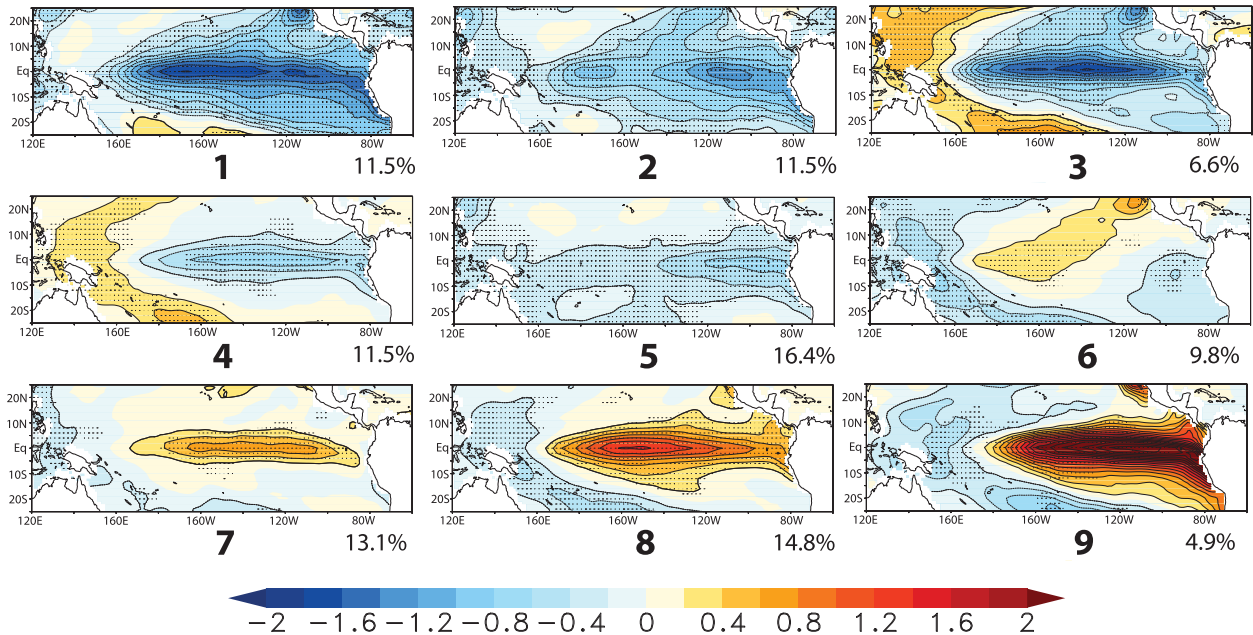


FIG. 2. The nine SST anomaly cluster patterns for a one-dimensional SOM. The contour interval is 0.2°C , with the zero contour omitted. Stippling indicates anomalies that are statistically significant at the 5% significance level. The percentages to the bottom right of each map refer to the frequency of occurrence of the pattern for the 1950–2011 period.

patterns occur with similar frequency. To verify that these nine patterns do, in fact, resemble the seasonal SST fields that comprise the clusters, centered pattern correlations (e.g., Santer et al. 1993) between each SST field and its corresponding best-matching SOM pattern are calculated. The mean pattern correlation is 0.76, which confirms the close resemblance between these nine patterns and the individual constituent SST anomaly fields of each cluster.

b. Changes in frequency distribution within the ENSO continuum

Next we examine how the frequency of occurrence of these nine SOM patterns has varied over the past 60 years and how these changes in frequency have influenced the long-term tropical Pacific SST trends. Figure 3 illustrates the occurrence time series for each of the nine patterns. This plot demonstrates that each SOM pattern generally occurs for a single season and for no more than two consecutive years. In addition, Fig. 3 indicates whether at least four of the six months in the September through February season are classified as an El Niño or La Niña episode by NOAA CPC. NOAA CPC classifies an El Niño (La Niña) episode when the three-month running mean Niño-3.4 SST anomaly is greater than 0.5°C ($< -0.5^{\circ}\text{C}$) for at least five consecutive overlapping, three-month seasons. Figure 3 confirms that patterns 1–4 are closely associated with La Niña episodes, and patterns

6–9 are tied to El Niño episodes. Pattern 5 generally occurs when neutral ENSO conditions are declared. The CP El Niño episodes noted in previous literature (e.g., Kug et al. 2009) generally correspond with SOM patterns 6 (e.g., 1977/78 and 1990/91), 7 (e.g., 2004/05), or 8

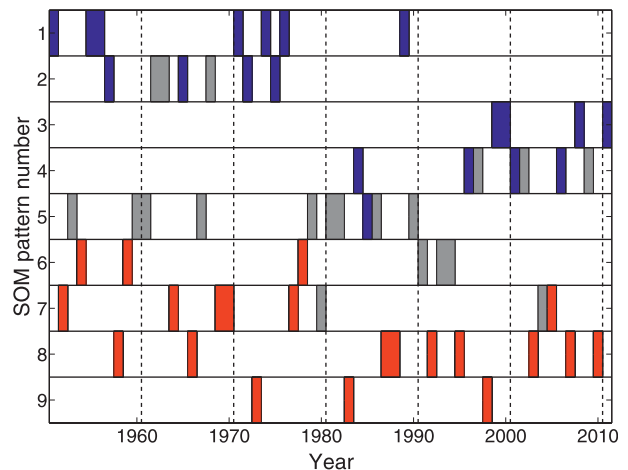


FIG. 3. Occurrence time series for each of the nine SOM patterns in Fig. 2 (the assigned year corresponds to that of January–February in the September–February season). Filled bars indicate pattern occurrence for the particular year. Red (blue) bars indicate the occurrence of an El Niño (La Niña) episode during at least four of the six months, and gray bars indicate the classification as an ENSO neutral season.

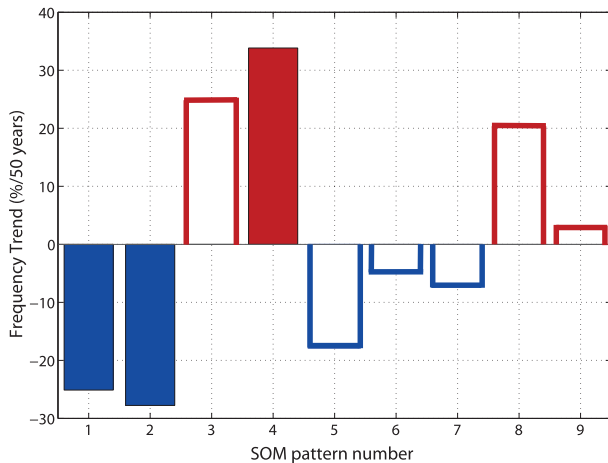


FIG. 4. Trends in the frequency of occurrence for each of nine SOM patterns in Fig. 2. Filled bars signify trends that are statistically significant at the 5% level with respect to a nine-state first-order Markov chain (see text for details).

(e.g., 1994/95 and 2002/03). The only clearly defined EP El Niño pattern, SOM pattern 9, corresponds with the strong El Niño episodes of 1972/73, 1982/83, and 1997/98. This observation that recent strong El Niño episodes have strongly positive SST anomalies centered in the eastern Pacific, but that all other El Niño episodes are centered over a broad range of longitudes is consistent with the recent studies of Giese and Ray (2011) and Ray and Giese (2012).

Perhaps the most striking feature of Fig. 3 is the obvious trend in patterns 1–4, with patterns 1 and 2 prevalent early in the period but nearly absent in the second half of the period, and patterns 3 and 4 prevalent only after the mid-1990s. This trend represents a transition from La Niña-like patterns with weak or negative SST anomalies in the western Pacific warm pool (patterns 1 and 2) to La Niña-like patterns with positive SST anomalies in the western Pacific warm pool (patterns 3 and 4).

This transition is demonstrated more clearly in Fig. 4, which shows the trend in the frequency of occurrence for each SOM pattern. Statistical significance is assessed with respect to a K -state first-order Markov chain, as determined through a Monte Carlo test similar to that of Riddle et al. (2013). For this test, 10 000 synthetic first-order Markov chain SOM pattern occurrence time series (like that of Fig. 3) are generated with the same transition probabilities as observed. For each synthetic time series the trend in pattern frequency of occurrence is calculated. Observed trends that are greater than the 97.5th or less than the 2.5th percentile of the synthetic trends are deemed statistically significant at the 5% level. Figure 4 confirms that the trends in SOM patterns 1–4 are strongest, with only the trend in pattern 3 falling

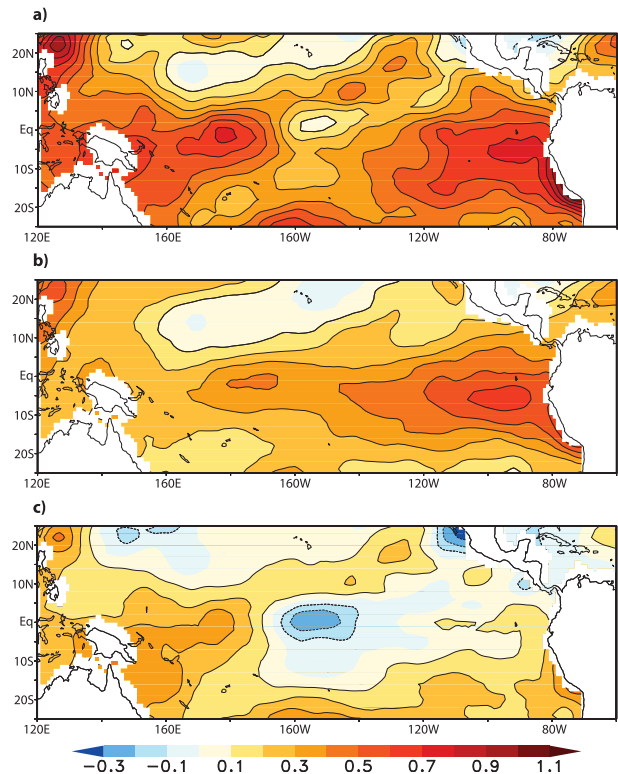


FIG. 5. (a) Total and (b) SOM-derived September–February SST trend [$^{\circ}\text{C} (50 \text{ yr})^{-1}$] for 1950–2011. (c) Difference between total and SOM-derived SST trends [(a) minus (b)]. The contour interval is $0.1^{\circ}\text{C} (50 \text{ yr})^{-1}$, and the zero contour line is omitted.

just short of statistical significance. Although flavors of El Niño have received more focus than those of La Niña, none of the trends in El Niño-like patterns (patterns 6–9) is statistically significant over the past 60 years.

To determine how these SOM pattern frequency trends have contributed to the total tropical Pacific SST trends, we calculate the SOM-derived trend as

$$\frac{d\text{SST}_{\text{SOM}}(\lambda, \theta)}{dt} = \sum_{i=1}^K \frac{df_i}{dt} \text{SST}_i(\lambda, \theta), \quad (4)$$

where df_i/dt is the frequency trend of SOM pattern i , and SST_i is SOM pattern i . Figure 5 presents the total and SOM-derived September–February SST trends over the tropical Pacific region. The total SST trend (Fig. 5a) reveals warming over the past 60 years over almost the entire domain, but the most pronounced warming is indicated over the eastern equatorial Pacific and western Pacific warm pool. The trend derived from (4) (Fig. 5b) also shows warming over most of the domain, but the warming is most pronounced only over the eastern Pacific region. Figure 4 suggests that most of these ENSO

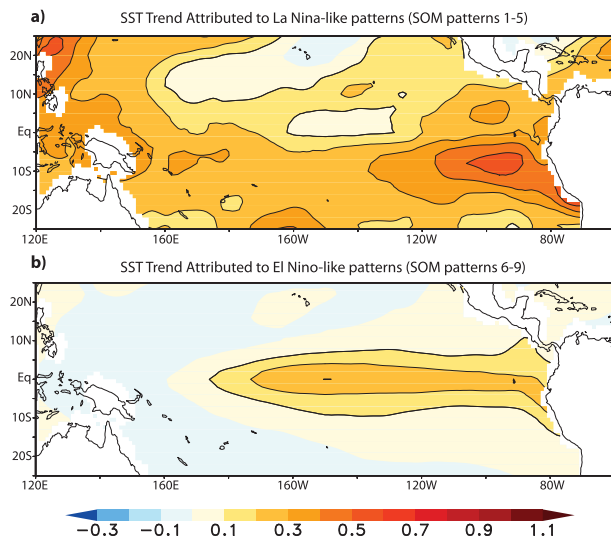


FIG. 6. As in Fig. 5b, but calculated only for (a) La Niña-like SOM patterns 1–5 and for (b) El Niño-like SOM patterns 6–9.

flavor-related trends relate to changes in the frequency of La Niña-like rather than El Niño-like patterns. This suggestion is confirmed in Fig. 6, which shows the trends from the application of (4) only for La Niña-like SOM patterns 1–5 (Fig. 6a) and only for El Niño-like SOM patterns 6–9 (Fig. 6b). The trend pattern derived solely from La Niña-like pattern frequency changes (Fig. 6a) closely resembles the total ENSO-related trend pattern (Fig. 5b). The positive trends in El Niño-like pattern frequencies have contributed to modest warming in the eastern equatorial Pacific region, but El Niño-related trends are weak throughout the rest of the domain (Fig. 6b).

The difference between the total and SOM-derived trends (Fig. 5c) reveals generally weak and even negative SST trends over the equatorial Pacific domain but with pronounced positive trends remaining over the western Pacific warm pool. This result suggests that trends in the frequency of occurrence of various ENSO flavors have dominated the SST trends in the eastern equatorial Pacific region, but the trends in the western Pacific warm pool reflect a combination of changes in frequency distribution and an additional superimposed long-term non-ENSO trend.

4. Discussion

The preceding analysis reveals nine statistically distinguishable patterns that represent the ENSO continuum. This continuum perspective contrasts the framework of recent studies that suggest two clearly distinct types of El Niño. This continuum perspective also is supported by the recent work of Giese and Ray (2011), who find

that the central longitude of El Niño SST anomalies is not bimodal but rather is indistinguishable from a Gaussian distribution centered near 140°W. One notable observation is that the three strongest El Niño episodes of the past 60 years as measured by Niño-3.4 SST anomalies (1972/73, 1982/83, and 1997/98) feature the strongest SST anomalies in the eastern Pacific (SOM pattern 9). Perhaps the increased attention paid to these strongest episodes has resulted in an overemphasis of the differences between EP and CP El Niño episodes. Evidence from an ocean reanalysis suggests that these strong EP El Niño episodes may have resulted in an eastward bias of reconstructed El Niño SST anomalies for periods before 1950 owing to the influence of these strong El Niño episodes on the SST reconstructions (Giese and Ray 2011; Ray and Giese 2012).

The analysis also reveals that these nine ENSO flavors have made a significant contribution to the long-term tropical Pacific SST trend through changes in their frequency distribution (Fig. 5b). The most significant trends relate to La Niña-like patterns, with the dominance of patterns with negative western Pacific SST anomalies (patterns 1 and 2) before the mid-1970s followed by the dominance of patterns with positive western Pacific SST anomalies (patterns 3 and 4) after the mid-1970s, particularly from the mid-1990s to the present. These frequency trends have contributed to tropical Pacific warming, particularly in the western Pacific and eastern equatorial Pacific regions (Fig. 6a). One may hypothesize that this behavior reflects a long-term warming trend most pronounced in the western Pacific warm pool superimposed on interannual ENSO variability. However, this analysis suggests that there is a disproportionate western Pacific warming for La Niña-like patterns, while there is no similar trend in the western Pacific evident for El Niño-like patterns.³ In fact, the positive trend in the frequency of El Niño-like patterns, particularly pattern 8, contributes to a weak *negative* SST trend in the western Pacific warm pool region (Fig. 6b). Therefore, this analysis suggests that the simple paradigm of a long-term trend superimposed on interannual variability, as typically assumed in global warming attribution studies (e.g., Pall et al. 2011), may not be sufficient for understanding tropical Pacific SST variability and trends. Rather, changes in the frequency distribution of interannually varying patterns within the ENSO continuum, as depicted in Fig. 2, may impart a significant contribution to the long-term trend. Moreover, recent theoretical

³ See Fig. 10 of L'Heureux et al. (2013) for additional evidence of enhanced western Pacific warm pool warming trends in La Niña episodes relative to El Niño episodes during November–February.

work (Liang et al. 2012) proposes that the recent elevation in ENSO variance may be more of a cause than a consequence of eastern tropical Pacific warming, which would further underscore the difficulty of separating interannual variability from the tropical mean state.

The trend toward La Niña-like patterns with positive SST anomalies in the western Pacific warm pool is of particular interest because this general pattern may represent the “perfect ocean for drought” over many midlatitude regions (Hoerling and Kumar 2003). This SST pattern, captured by SOM patterns 3 and 4, dominated during the period between 1998 and 2002 (Fig. 3), which was a period of prolonged drought throughout much of the United States, southern Europe, and southwest Asia. Climate model simulations suggest that both the negative SST anomalies in the eastern Pacific and positive SST anomalies in the western tropical Pacific acted synergistically to force the persistent drought during this period (Hoerling and Kumar 2003; Lau et al. 2006). Figure 3 reveals that SOM patterns 3 and 4 occurred several additional times since that period. In addition, there is evidence that the positive trend in Indo-Pacific warm pool SSTs has contributed to changes in the wintertime teleconnection response to La Niña, a trend toward a more zonally oriented circumglobal teleconnection pattern (Kumar et al. 2010; Lee et al. 2011). Given the widespread societal impacts of these particular La Niña flavors, it is worthwhile for future studies to investigate whether the disproportionate warm pool warming for La Niña-like patterns will continue.

Both an EP (pattern 9) and CP-EP El Niño (pattern 8) SOM pattern also have experienced positive trends in the frequency of occurrence over the past 60 years, but these trends are indistinguishable from natural variability (Fig. 4). Given the recent focus on whether CP El Niño episodes will become more frequent under global warming (Yeh et al. 2009), the positive trend of CP El Niño-like SOM pattern 8 is of particular interest. However, the lack of a significant trend is consistent with recent studies based on long integrations of a multivariate red noise model (Newman et al. 2011b) and a coupled climate model (Yeh et al. 2011), which found that the recent multidecadal increase in CP El Niño relative to EP El Niño episodes is consistent with natural variability.

The changes in frequency of the ENSO flavor SOM patterns have contributed to an overall positive SST trend in the central and eastern equatorial Pacific region (Fig. 5b), which is consistent with recent findings linking positive equatorial Pacific trends to ENSO (Compo and Sardeshmukh 2010; Lee and McPhaden 2010; L’Heureux et al. 2013). In addition, the increased dominance of SOM patterns 3 and 4 at the expense of patterns 1 and 2 has contributed to the warming trend in

the tropical western Pacific region. The residual SST trend (Fig. 5c) reveals positive SST trends in the western Pacific but weak or even negative SST trends throughout the equatorial eastern Pacific region. Interestingly, this residual trend in Fig. 5c is somewhat similar to the ENSO-unrelated SST trends obtained after applying a dynamic ENSO filter (Compo and Sardeshmukh 2010; Solomon and Newman 2012). This particular filter, which accounts for the SST evolution during ENSO and is obtained through a linear inverse modeling approach, reveals a trend pattern of western Indo-Pacific warming and eastern equatorial Pacific cooling after the trends associated with ENSO have been removed. The approach adopted here similarly shows that ENSO-related trends have contributed to eastern equatorial Pacific warming (Fig. 5b), and the residual SST warming is most pronounced in the western Pacific warm pool (Fig. 5c). However, we must exercise caution when viewing long-term SST trends, given the data uncertainties. In particular, a recent SST reconstruction based only on bucket SST and nighttime marine surface air temperature measurements suggests less pronounced western Pacific warming relative to that of the eastern Pacific (Tokinaga et al. 2012). Although beyond the scope of this study, future research will continue to investigate whether this enhanced western Pacific warming is real, and, if so, whether it represents a response to anthropogenic warming (Clement et al. 1996; Cane et al. 1997) or if enhanced equatorial Pacific warming, as in global climate models (Collins et al. 2010; Xie et al. 2010), is more likely. The interplay between the potential impact of greenhouse gas warming on ENSO (Guilyardi et al. 2009; Yeh et al. 2009; Collins et al. 2010; Vecchi and Wittenberg 2010) and on long-term SST trends is a challenging problem, but the approach presented here provides a possible framework for exploring this interaction.

5. Conclusions

This study opens with this question: How many ENSO flavors can we distinguish? To address this question, we examine an approach that partitions tropical Pacific SST fields through SOM analysis and then determines the maximum number of SOM cluster patterns that are statistically distinguishable. This approach can be applied more generally to other cluster analysis problems, particularly those of *K*-means cluster or SOM analysis, in order to answer the recurring question of what is the optimal, or at least the maximum, number of clusters to retain. The approach adopted here has the appeal of being grounded in an accessible concept, statistical distinguishability. Many other applications with serially correlated data would face the additional challenge of

accounting for serial correlation in the calculation of local p values, but the basic approach described here still would apply.

Although the present study focuses on seasonal SST patterns, ENSO also undergoes other types of interdecadal variations, including changes in the seasonal evolution of ENSO-related SST anomalies. Future extensions of this study may explore seasonal variations of ENSO flavors. In addition, the dynamical processes responsible for these nine patterns remain an open question. Through a multivariate red noise framework for tropical SST variability, Newman et al. (2011a,b) find that the leading optimal structure corresponding with the EP ENSO is driven by both surface and thermocline interactions, as in the classic “recharge–discharge” mechanism (Jin 1997). In contrast, the optimal structure corresponding with CP ENSO evolves through nonlocal SST interactions, such as the advection of SST anomalies, but without the recharge–discharge mechanism. The CP ENSO event growth is more modest than that of the EP ENSO, but the lack of a discharge mechanism allows the CP ENSO to decay more slowly (Newman et al. 2011b). Because these two optimal initial structures are orthogonal, the framework of Newman et al. (2011a,b) suggests a continuum of “mixed” CP–EP ENSO patterns with intermediate dynamical characteristics. The analysis presented here is consistent with this general framework, but additional work is needed.

The analysis presented here also suggests that although El Niño flavors often receive more focus than those of La Niña in the literature, changes related to La Niña–like SST patterns have made a stronger impact on long-term SST trends over the past 60 years. A number of outstanding questions remain. Given that tropical Pacific SST anomalies have far-reaching effects through tropical convection anomalies and the triggering of atmospheric teleconnections, future research shall augment recent efforts (e.g., Larkin and Harrison 2005; Weng et al. 2007; Mo 2010; Hu et al. 2012) to examine how many ENSO flavor teleconnections and remote impacts can be distinguished. In addition, the various ENSO flavors within the ENSO continuum and their relationship with the long-term SST trend remain an active area of research (Guilyardi et al. 2009; Yeh et al. 2009; Collins et al. 2010; Liang et al. 2012). A unique set of questions raised in this study relates to the trend toward La Niña–like patterns with enhanced SST anomalies in the western Pacific warm pool. Why has there been disproportionate western Pacific warming for La Niña patterns? Will this trend continue? Can coupled global climate models capture this sort of variability? The approach presented here provides a framework for examining the ENSO continuum and questions like

these with a manageable set of representative ENSO flavors.

Acknowledgments. I sincerely thank Drs. Steven Feldstein, Sukyoung Lee, Jinbao Li, and Shang-Ping Xie for thoughtful discussions and helpful comments that contributed to this work. I also thank Dr. Eli Tziperman and two anonymous reviewers for constructive comments that improved the quality of this study. I am grateful for support through a grant from the NOAA Climate Test Bed program. NOAA ERSST.v3 data are provided by the NOAA/OAR/ESRL PSD, Boulder, Colorado, USA, from their Web site at <http://www.esrl.noaa.gov/psd>.

REFERENCES

- Ashok, K., S. K. Behera, S. A. Rao, H. Weng, and T. Yamagata, 2007: El Niño Modoki and its possible teleconnection. *J. Geophys. Res.*, **112**, C11007, doi:10.1029/2006JC003798.
- Benjamini, Y., and Y. Hochberg, 1995: Controlling the false discovery rate: A practical and powerful approach to multiple testing. *J. Roy. Stat. Soc.*, **B57**, 289–300.
- Cane, M. A., A. C. Clement, A. Kaplan, Y. Kushnir, D. Pozdnyakov, R. Seager, S. E. Zebiak, and R. Murtugudde, 1997: Twentieth-century sea surface temperature trends. *Science*, **275**, 957–960.
- Christiansen, B., 2007: Atmospheric circulation regimes: Can cluster analysis provide the number? *J. Climate*, **20**, 2229–2250.
- Chu, J.-E., S. N. Hameed, and K.-J. Ha, 2012: Non-linear, intra-seasonal phases of the East Asian summer monsoon: Extraction and analysis using self-organizing maps. *J. Climate*, **25**, 6975–6988.
- Clement, A. C., R. Seager, M. A. Cane, and S. E. Zebiak, 1996: An ocean dynamical thermostat. *J. Climate*, **9**, 2190–2196.
- Collins, M., and Coauthors, 2010: The impact of global warming on the tropical Pacific Ocean and El Niño. *Nat. Geosci.*, **3**, 391–397.
- Compo, G. P., and P. D. Sardeshmukh, 2010: Removing ENSO-related variations from the climate record. *J. Climate*, **23**, 1957–1978.
- Deser, C., M. A. Alexander, S.-P. Xie, and A. S. Phillips, 2010: Sea surface temperature variability: Patterns and mechanisms. *Annu. Rev. Mar. Sci.*, **2010** (2), 115–143.
- Folland, C., and C. Anderson, 2002: Estimating changing extremes using empirical ranking methods. *J. Climate*, **15**, 2954–2960.
- Freeman, L. A., A. J. Miller, R. D. Norris, and J. E. Smith, 2012: Classification of remote Pacific coral reefs by physical oceanographic environment. *J. Geophys. Res.*, **117**, C02007, doi:10.1029/2011JC007099.
- Giese, B. S., and S. Ray, 2011: El Niño variability in simple ocean data assimilation (SODA), 1871–2008. *J. Geophys. Res.*, **116**, C02024, doi:10.1029/2010JC006695.
- Guilyardi, E., A. Wittenberg, A. Fedorov, M. Collins, C. Wang, A. Capotondi, G. J. van Oldenborgh, and T. Stockdale, 2009: Understanding El Niño in ocean–atmosphere general circulation models: Progress and challenges. *Bull. Amer. Meteor. Soc.*, **90**, 325–340.
- Hastie, T., R. Tibshirani, and J. Friedman, 2009: Unsupervised learning. *The Elements of Statistical Learning: Data Mining, Inference, and Prediction*, Springer, 485–585.

- Hewitson, B. C., and R. G. Crane, 2002: Self-organizing maps: Applications to synoptic climatology. *Climate Res.*, **22**, 13–26.
- Hoerling, M. P., and A. Kumar, 2003: The perfect ocean for drought. *Science*, **299**, 691–694.
- , —, and M. Zhong, 1997: El Niño, La Niña, and the non-linearity of their teleconnections. *J. Climate*, **10**, 1769–1786.
- Hu, Z.-Z., A. Kumar, B. Jha, W. Wang, B. Huang, and B. Huang, 2012: An analysis of warm pool and cold tongue El Niños: Air–sea coupling processes, global influences, and recent trends. *Climate Dyn.*, **38**, 2017–2035, doi:10.1007/s00382-011-1224-9.
- Jin, B., G. Wang, Y. Liu, and R. Zhang, 2010: Interaction between the East China Sea Kuroshio and the Ryukyu Current as revealed by the self-organizing map. *J. Geophys. Res.*, **115**, C12047, doi:10.1029/2010JC006437.
- Jin, F.-F., 1997: An equatorial ocean recharge paradigm for ENSO. Part I: Conceptual model. *J. Atmos. Sci.*, **54**, 811–829.
- Johnson, N. C., and S. B. Feldstein, 2010: The continuum of North Pacific sea level pressure patterns: Intraseasonal, interannual, and interdecadal variability. *J. Climate*, **23**, 851–867.
- , and S.-P. Xie, 2010: Changes in the sea surface temperature threshold for tropical convection. *Nat. Geosci.*, **3**, 842–845.
- , S. B. Feldstein, and B. Tremblay, 2008: The continuum of Northern Hemisphere teleconnection patterns and a description of the NAO shift with the use of self-organizing maps. *J. Climate*, **21**, 6354–6371.
- Kao, H.-Y., and J.-Y. Yu, 2009: Contrasting eastern-Pacific and central-Pacific types of ENSO. *J. Climate*, **22**, 615–632.
- Kohonen, T., 2001: *Self-Organizing Maps*. Springer, 501 pp.
- Kug, J.-S., F.-F. Jin, and S.-I. An, 2009: Two types of El Niño events: Cold tongue El Niño and warm pool El Niño. *J. Climate*, **22**, 1499–1515.
- Kumar, A., B. Jha, and M. L’Heureux, 2010: Are tropical SST trends changing the global teleconnection during La Niña? *Geophys. Res. Lett.*, **37**, L12702, doi:10.1029/2010GL043394.
- Larkin, N. K., and D. E. Harrison, 2005: Global seasonal temperature and precipitation anomalies during El Niño autumn and winter. *Geophys. Res. Lett.*, **32**, L16705, doi:10.1029/2005GL022860.
- Lau, N.-C., A. Leetmaa, and M. J. Nath, 2006: Attribution of atmospheric variations in the 1997–2003 period to SST anomalies in the Pacific and Indian Ocean basins. *J. Climate*, **19**, 3607–3628.
- Lee, S., T. Gong, N. Johnson, S. B. Feldstein, and D. Pollard, 2011: On the possible link between tropical convection and the Northern Hemisphere Arctic surface air temperature change between 1958 and 2001. *J. Climate*, **24**, 4350–4367.
- Lee, T., and M. J. McPhaden, 2010: Increasing intensity of El Niño in the central-equatorial Pacific. *Geophys. Res. Lett.*, **37**, L14603, doi:10.1029/2010GL044007.
- Leloup, J., Z. Lachkar, J.-P. Boulanger, and S. Thiria, 2007: Detecting decadal changes in ENSO using neural networks. *Climate Dyn.*, **28**, 147–162, doi:10.1007/s00382-006-0173-1.
- L’Heureux, M. L., D. C. Collins, and Z.-Z. Hu, 2013: Linear trends in sea surface temperature of the tropical Pacific Ocean and implications for the El Niño–Southern Oscillation. *Climate Dyn.*, **40**, 1223–1236, doi:10.1007/s00382-012-1331-2.
- Liang, J., X.-Q. Yang, and D.-Z. Sun, 2012: The effect of ENSO events on the tropical Pacific mean climate: Insights from an analytical model. *J. Climate*, **25**, 7590–7606.
- Liu, Y., R. H. Weisberg, and C. N. K. Mooers, 2006: Performance evaluation of the self-organizing map for feature extraction. *J. Geophys. Res.*, **111**, C05018, doi:10.1029/2005JC003117.
- Livezey, R. E., and W. Y. Chen, 1983: Statistical field significance and its determination by Monte Carlo techniques. *Mon. Wea. Rev.*, **111**, 46–59.
- Ma, J., S.-P. Xie, and Y. Kosaka, 2012: Mechanisms for tropical tropospheric circulation change in response to global warming. *J. Climate*, **25**, 2979–2993.
- Michelangeli, P.-A., R. Vautard, and B. Legras, 1995: Weather regimes: Recurrence and quasi stationarity. *J. Atmos. Sci.*, **52**, 1237–1256.
- Mo, K., 2010: Interdecadal modulation of the impact of ENSO on precipitation and temperature over the United States. *J. Climate*, **23**, 3639–3656.
- Newman, M., M. A. Alexander, and J. D. Scott, 2011a: An empirical model of tropical ocean dynamics. *Climate Dyn.*, **37**, 1823–1841.
- , S.-I. Shin, and M. A. Alexander, 2011b: Natural variation in ENSO flavors. *Geophys. Res. Lett.*, **38**, L14705, doi:10.1029/2011GL047658.
- Pall, P., T. Aina, D. A. Stone, P. A. Stott, T. Nozawa, A. G. J. Hilberts, D. Lohmann, and M. R. Allen, 2011: Anthropogenic greenhouse gas contribution to flood risk in England and Wales in autumn 2000. *Nature*, **470**, 382–385.
- Ray, S., and B. S. Giese, 2012: Historical changes in El Niño and La Niña characteristics in an ocean reanalysis. *J. Geophys. Res.*, **117**, C11007, doi:10.1029/2012JC008031.
- Reusch, D. B., R. B. Alley, and B. C. Hewitson, 2005: Relative performance of self-organizing maps and principal component analysis in pattern extraction from synthetic climatological data. *Polar Geogr.*, **29**, 227–251.
- Richardson, A. J., C. Risien, and F. A. Shillington, 2003: Using self-organizing maps to identify patterns in satellite imagery. *Prog. Oceanogr.*, **59**, 223–239.
- Riddle, E. E., M. B. Stoner, N. C. Johnson, M. L. L’Heureux, D. C. Collins, and S. B. Feldstein, 2013: The impact of the MJO on clusters of wintertime circulation anomalies over the North American region. *Climate Dyn.*, **40**, 1749–1766, doi:10.1007/s00382-012-1493-y.
- Rodgers, K. B., P. Friederichs, and M. Latif, 2004: Tropical Pacific decadal variability and its relation to decadal modulation of ENSO. *J. Climate*, **17**, 3761–3774.
- Ropelewski, C. F., and M. S. Halpert, 1987: Global and regional scale precipitation patterns associated with the El Niño/Southern Oscillation. *Mon. Wea. Rev.*, **115**, 1606–1626.
- Santer, B. D., T. M. L. Wigley, and P. D. Jones, 1993: Correlation methods in fingerprint detection studies. *Climate Dyn.*, **8**, 265–276.
- Shin, S.-I., and P. D. Sardeshmukh, 2011: Critical influence of the pattern of tropical ocean warming on remote climate trends. *Climate Dyn.*, **36**, 1577–1591.
- Smith, T. M., R. W. Reynolds, T. C. Peterson, and J. Lawrimore, 2008: Improvements to NOAA’s historical merged land–ocean surface temperature analysis (1880–2006). *J. Climate*, **21**, 2283–2296.
- Solomon, A., and M. Newman, 2012: Reconciling disparate twentieth-century Indo-Pacific ocean temperature trends in the instrumental record. *Nat. Climate Change*, **2**, 691–699, doi:10.1038/nclimate1591.
- Tokinaga, H., S.-P. Xie, C. Deser, Y. Kosaka, and Y. M. Okumura, 2012: Slowdown of the Walker circulation driven by tropical Indo-Pacific warming. *Nature*, **491**, 439–443.
- Trenberth, K. E., and J. M. Caron, 2000: The Southern Oscillation revisited: Sea level pressures, surface temperatures, and precipitation. *J. Climate*, **13**, 4358–4365.

- , and D. P. Stepaniak, 2001: Indices of El Niño evolution. *J. Climate*, **14**, 1697–1701.
- Vecchi, G. A., and A. T. Wittenberg, 2010: El Niño and our future climate: Where do we stand? *Wiley Interdiscip. Rev.: Climate Change*, **1**, 260–270.
- Vesanto, J., J. Himberg, E. Alhoniemi, and J. Parhankangas, cited 2000: SOM toolbox for Matlab 5. Helsinki University of Technology, Finland. [Available online at <http://www.cis.hut.fi/projects/somtoolbox/>.]
- Weng, H., K. Ashok, S. K. Behera, S. A. Rao, and T. Yamagata, 2007: Impacts of recent El Niño Modoki on dry/wet conditions in the Pacific Rim during boreal summer. *Climate Dyn.*, **29**, 113–129.
- Wilks, D. S., 2006: On “field significance” and the false discovery rate. *J. Appl. Meteor. Climatol.*, **45**, 1181–1189.
- Xie, S.-P., C. Deser, G. A. Vecchi, J. Ma, H. Teng, and A. T. Wittenberg, 2010: Global warming pattern formation: Sea surface temperature and rainfall. *J. Climate*, **23**, 966–986.
- Xue, Y., T. M. Smith, and R. W. Reynolds, 2003: Interdecadal changes of 30-yr SST normals during 1871–2000. *J. Climate*, **16**, 1601–1612.
- Yeh, S.-W., J.-S. Kug, B. Dewitte, M.-H. Kwon, B. P. Kirtman, and F.-F. Jin, 2009: El Niño in a changing climate. *Nature*, **461**, 511–514.
- , B. K. Kirtman, J.-S. Kug, W. Park, and M. Latif, 2011: Natural variability of the central Pacific El Niño event on multi-centennial timescales. *Geophys. Res. Lett.*, **38**, L02704, doi:10.1029/2010GL045886.
- Yu, J.-Y., and S. T. Kim, 2011: Relationships between extratropical sea level pressure variations and the central Pacific and eastern Pacific types of ENSO. *J. Climate*, **24**, 708–720.